MHD Activity during ELMs

S.von Goeler[+], O.Klüber, G.Fußmann, J.Gernhardt,
M.Kornherr

IPP III/143 Januar 1989

MAX-PLANCK-INSTITUT FÜR PLASMAPHYSIK

8046 GARCHING BEI MÜNCHEN

MAX-PLANCK-INSTITUT FÜR PLASMAPHYSIK

GARCHING BEI MÜNCHEN

MHD Activity during ELMs

S.von Goeler[+], O.Klüber, G.Fußmann, J.Gernhardt,
M.Kornherr

IPP III/143 Januar 1989

Die nachstehende Arbeit wurde im Rahmen des Vertrages zwischen dem Max-Planck-Institut für Plasmaphysik und der Europäischen Atomgemeinschaft über die Zusammenarbeit auf dem Gebiete der Plasmaphysik durchgeführt.

MHD Activity during ELMs

S.von Goeler*, O.Klüber, G.Fußmann, J.Gernhardt, M.Kornherr

Max Planck Institut für Plasmaphysik,

D-8046 Garching bei München, Germany

Abstract

The MHD activity has been monitored in the ASDEX tokamak during ELMs. Besides a fast inward shift of the plasma column, a helical MHD perturbation has been found to accompany every ELM. In general the helical instability has an m number of 3 or 4, an n number of 1, and it propagates in the direction of the electron diamagnetic drift. It seems to be identical with the Toi mode, which had been observed[1] to disappear during L to H transitions.

Introduction

In the ASDEX tokamak during periods of improved H-mode[2] confinement, an instability has been observed, the so called Edge-Localized-Mode (ELM)[3], which is characterized by a sudden increase in the emission of Hα light in the divertor, a rapid decline of the soft X-ray emission from the plasma boundary, and a fast decrease of the poloidal Beta. A similar behavior of these signals is seen on ASDEX during transitions from the L mode to the H mode, and ELMs are consequently considered by some researchers to be short H-L-H transitions, although the Hα signal and the plasma

---

* On leave from the Plasma Physics Laboratory, Princeton University, Princeton, N.J 08543, USA

losses during ELMs are in general much larger than during the L phase[4]. The physical causes behind phenomena like the L-H transition, the H-L transition, or the ELM are presently unknown, and it seems that a detailed study of the ELMs would be specially suited to shed some light on the underlying physics. The purpose of the present paper is to report the results of an investigation of the MHD activity during ELMs on ASDEX. We find that all ELMs are accompanied by a strong inward shift and by helical m=3 or m=4 instabilities. Recently, K.Toi et al. have investigated the MHD activity during L-H transitions[1], and have found an MHD instability on the Mirnov coil signals, which seems to be present during the L phase of most discharges and to disappear during the H phase. The helical instabilities that are observed during the ELMs seem to be identical with the Toi mode. Helical instabilities during ELMs have also been observed on PDX [5] and on DIII-D [6].

The quality of H-mode phases of ASDEX discharges seems to be closely correlated with the frequency of ELMs. The highest values of the poloidal beta and of the confinement time are obtained in those H-mode discharges in which there exists a long time period which is free from ELMS. This time period is usually followed by a time interval in which periodic, single ELMs occur; these ELMs increase in frequency, until, finally, the H-L transition occurs. On the other hand, very little improvement in confinement is observed in H-mode discharges, in which ELMs are very frequent and where the Hα signal consequently has a kind of "grassy" appearance. As far as MHD measurements are concerned, the two types of discharges differ in that the plasma inward motion accounts for the dominating part of the Mirnov signals in single ELM discharges, whereas the helical instability seems to be the most prominent feature in discharges with grassy ELMs. Therefore, we shall first discuss the plasma motion during single ELMs, then the helical instability during grassy ELMs, and finally the helical instability during single ELMs.

Plasma Motion during Single ELMs.

Typical traces of the Hα emission, the soft X-ray emission near the plasma edge, and the B_θ signal from a coil located in the midplane on the outside of the torus are shown in Fig. 1 for a discharge with single ELMs. In the course of this discharge, the plasma had gone into the H mode at an earlier time (t = 1.08 s), it had then lived through an ELM free time period of about 65 ms, and it is now in the phase where single ELMs occur with increasing frequency, until the plasma undergoes an H-L transition at time t= 1.207 s. The ELMs are clearly visible as spikes on the Hα traces, and as downward steps on the soft X-ray emission from the plasma edge. All the outer Mirnov coils with major radius R larger then the plasma major radius R_o exhibit negative spikes at the time when the ELM occurs, whereas all inside coils, $R < R_o$, show positive spikes. This observation shows that an inward motion of the plasma takes place. In Fig. 2 we show the signals from four Mirnov coils, that are located on a circle around the plasma at poloidal angles $\theta = 51^o, -51^o, 149.4^o$, and -149.4^o, on an enlarged time scale. (The poloidal angle θ is measured from the midplane starting on the outside of the torus in the mathematically positive sense). The figure illustrates that the spikes are indeed positive for the inside coils and negative for the outside coils. In addition it shows that an oscillatory motion occurs, which is ascribed to an instability. This helical instability will be analyzed further below.

The horizontal motion of the plasma can be deduced from the Mirnov traces in an approximate fashion by interpreting the signals as the result of a displacement of the current channel. This procedure neglects changes of the vertical magnetic field. However, the vertical field is smaller than B_θ by the aspect ratio, and the procedure is, therefore, considered to be approximately correct. The

result for the ELM of Fig.2 is shown in Fig. 3. The displacement is particularly large for this ELM. In general we find that the plasma moves by a few mm during an ELM. The horizontal motion is comparatively slow, slower for instance than the decay of the soft X-ray signals from the plasma edge. The signals shown here are from the vertical X-ray camera, and they are consequently sensitive to horizontal motions; however the signals from the horizontal X-ray camera behave in similar fashion.

There are indications that also a vertical motion of the plasma occurs, which, however, seems to be an oscillatory up-down motion with frequency comparable to the helical instability.

Helical Instability during grassy ELMs.

The structure of the helical perturbation is most evident on the Mirnov signal traces during grassy ELMs. A typical discharge with grassy ELMs is shown in Fig.4. The Hα emission of this discharge exhibits many spikes which sometimes cluster and overlap. For instance at time t = 1.054 s the ELMs cluster for a time span of almost 3 ms; in fact this feature almost looks like a short L-H-L transition. It is during such ELM clusters that the helical perturbations are most clearly seen. As will be discussed later, helical perturbations seem to be present during all ELMs, but their structure is very often hidden behind other phenomena that also produce signals on the Mirnov loops. Such phenomena are, for instance, the horizontal and vertical motions, that we have discussed previously. In addition, there are internal MHD instabilities which produce signals on the Mirnov loops, for instance m=2 instabilities or higher-m satellite oscillations that are driven through toroidal coupling by m =1 modes.[7] The oscillations seen in Fig.4 from 1.045 to 1.050 s or in Fig.1 around time t = 1.150 s are typical examples. The satellite oscillations, however, tend to have a higher frequency, and they can usually be separated out by smoothing. Of course, the most simple way to avoid interference is to study ELMS at time

intervals in which no other instabilities are present.

Detailed B_θ-loop traces during the cluster-ELM of Fig.4 are presented in Figs.5. We will show now that modeling of the traces identifies the m number as 3. The traces have been smoothed by boxcar integration to eliminate the remnants of a small satellite oscillation. Modeling curves have been fitted by eye to the experimental traces. They have been calculated assuming that a sinusoidal m=3, n=1 helical perturbation propagates in the direction of the electron diamagnetic drift and grows and decays exponentially. In order to accommodate the so-called Merezhkin correction[8], the poloidal angle for the location of the probes was changed in the computation to correspond to the local rotational transform at the radius r_w, where the instability occurs.. (Physically, the coils are evenly spaced in a poloidal angle interval of $0^o \pm 51^o$ for the outer loops and $180^o \pm 30.6^o$ for the inner loops. The Merezhkin-corrected angles are noted in the figure.) In practice we found that the Merezhkin correction - making use of the measured value for $\beta_{pol} + l_i/2$ and a distance of 40 cm for the radius r_w - produced an over-correction. When we used a smaller value of $\beta_{pol} + l_i/2$, for instance two thirds of the measured value, we obtained satisfactory agreement with the experiment. We have no explanation for this fact. There is, however, little doubt that the m number is assigned correctly, because no reasonable fit can be made for the other possible odd modes, the m=1 and the m=5 mode. Besides the mode number m=3, we have observed - in particular for older data from the pre-1988 "unhardened" ASDEX - a mode-number of m=4 for the helical instability associated with ELMs.

The direction of propagation of this mode is in the direction of the electron diamagnetic drift. This behavior is very different from the behavior of the satellite modes that are driven by internal modes; the latter modes usually propagate in the direction of the beam-induced plasma rotation velocity[7], which for co-injection is in

the direction opposite to the electron diamagnetic drift direction. Since the central rotation velocity for the high power H-mode discharges tends to be much larger than the electron drift velocity, the frequency of the satellite oscillations is much higher than the frequency of the helical instability associated with ELMs. Because of these two observations - namely the fact that the mode number ratio m/n corresponds to the safety factor q near the plasma boundary, and the fact that the instability seems to propagate in a medium where the rotation velocity is zero or very small - we believe that the helical instability associated with the ELMs is located very near the outer edge of the plasma. Both facts are also characteristic for the Toi mode[1], and we believe, therefore, that the two modes are identical. It was also attempted to locate the mode on the soft X-ray traces, e.g. on traces like the ones shown in Figs.3c,3d, or 3e, in order to determine the radial extent of the helical instability. These attempts were not successful. For the case of single ELMs, there are frequency components in the correct frequency range on the soft X-ray traces, as Fig.3c,3d and 3e demonstrate. However the traces are too irregular to establish a definitive and reproducible correlation with B_θ-loop data. On the other hand during grassy ELMs, where the helical instability on the Mirnov loops is very regular, the X-ray intensity is too weak to perform fluctuation measurements. What the X-ray traces during single ELMs clearly show are the features of a disruptive process right at the plasma boundary, a process that transports hot plasma from the inside across the separatrix to the outside. This is illustrated in Fig.3, where the sudden fall-off of the X-ray traces for r =32.8 cm and 38.5 cm at time t= 1.18590 s, and the sudden rise of the X-ray traces for radius r = 40.3 cm and time t = 1.18590 s and the somewhat later rise for radius r = 38.5 cm at time 1.18593 s, is interpreted as the result of a fast heat transport. The behavior of the outer soft X-ray traces during ELMs resembles, in this respect, very closely the behavior that is observed on the inner soft X-ray traces during internal disruptions.

Another typical feature of the helical instability can be deduced

from the data of Figs.5a from a comparison of the amplitude of the experimental traces with the amplitude of the modeling curves: the amplitude of the oscillation is nearly the same for all probes. The amplitude is sometimes slightly smaller on the inside Mirnov coils, but not by a large factor, and some of the observed variations might result from the Shafranov shift or from the vertical shift of the plasma which is intentionally induced in order to facilitate the H transition. An exception to this rule is only exhibited by the trace of the Mirnov coil A11SST, where the experimental signal has an amplitude that is about two times larger than that of the other coils. This Mirnov coil is actually the loop located closest to the stagnation point of the divertor. The signal of this coil has tended to be larger than the rest in many (but not in all) instances. We have no explanation for this fact, and do not know whether it is of significance.

Helical Instability during single ELMs.

The presence of an inward motion during single ELMs tends to mask the Toi mode, which is the reason why the instability has previously gone unnoticed on ASDEX. However, we believe that the Toi mode is also present during all single ELMs. In order to better identify it, we have written a computer program which subtracts the horizontal plasma motion from the Mirnov traces. For this purpose we have added the negative average of the outer loops and the average of the inner loops, and assume that the sum signal represents the effects of the horizontal plasma motion. This procedure is not quite satisfactory because it does not properly distinguish between m = 1, m = 2, m = 3, and higher components. However, with the ASDEX B_θ-loop array, the cosine components of m=1 perturbations make up most of the signal, whereas the even-m cosine components are averaged out by inside and outside loops. Also the m = 3 and higher odd-m cosine components tend to become averaged out, because the range in poloidal angle θ_{max} which these coils occupy is larger than π/m. (This

condition is actually not too well fulfilled for the inside coils in case m=3). Finally all sine components are averaged out because of the up down symmetry of the arrays. [In an attempt to improve the data analysis, a computer program was written, which performed a kind of Fourier analysis. However, the results from the Fourier analysis were in general not very satisfactory: errors that were produced by small variations of the mode amplitude with poloidal angle θ have tended to create spurious higher-m components.] Results from the computer program employing the averaging and subtraction procedure are shown in FIGs.6 and Figs.7. The solid curves in Fig.6 represent the original experimental B_θ-loop data for a single ELM. The dashed curves are identical in all the various graphs of Fig.6; they are the averaged signal reflecting the horizontal motion. We find that the averaged signals describe the mean behavior quite well. The solid lines in Fig.7 are the difference signals (original B_θ-loop data minus averaged signal). The dashed lines in Figs.7 are modeling curves, similar to the ones discussed in Fig.5. The modeling suggests that a fast growing m=4, n=1 Toi mode is present at the onset of the ELM and lasts approximately up to time t = 1.1859 ms. We point out that the agreement between the modeling curves and the data is only marginal. Obvious discrepancies exist for the inner loops at the angles $\theta = -134.6^o$ to -180^o, and for the toroidal loops for $\phi = 134^o$. It is clear that the subtraction procedure tends to introduce errors which might be responsible for some of the discrepancies. However, the discrepancies have been present in almost all shots; in some, the agreement is better and in others it is even worse. The agreement seems to improve for ELMs that are weaker and that last longer; in fact there seems to be a steady transition from the irregular behavior observed during single ELMs to the very well defined helical modes observed in cluster ELMs (Figs.5). This observation provides the strongest argument for the hypothesis that both phenomena are the same or are at least very similar. After time t = 1.1859 s, very severe discrepancies between the modeling curves and the experimental traces appear, which suggest that a non-linear development sets in.

It is an open question whether there is a real change in the evolution of the instability, or whether the irregularities are caused by the rapid deterioration of plasma profiles near the plasma boundary. It seems, however, that not only the frequency of the mode, but also its character (mode number etc.) changes. The instability is characterized in this later stage by a very erratic behavior which varies from ELM to ELM, and we have not been able to establish a fixed pattern for the development of the instability during this phase. It seems that this change in mode character was also observed on PDX [5].

In the temporal evolution of an ELM (Figs.8a - 8f), the onset of the Toi mode precedes the fast rise of the Hα emission in the divertor by approximately 50 μs, but it is practically simultaneous with the decay of the soft X-ray signals from the plasma edge or with the fast rise of various carbon or oxygen impurity lines that are emitted near the plasma boundary. The observed time development, consequently, does not permit one to decide, whether the helical instability plays an active part in driving an ELM, or is just a feature that accompanies a disruptive process at the plasma edge that is caused by another physical mechanism. The size of the magnetic field perturbation at the location of the Mirnov loop is typically a fraction of a Gauss, for instance about 1/3 Gauss for the instability depicted in Figs. 7. An MHD instability with such small magnetic field seems to be at the limit where a mode can affect the plasma through island formation and ergodization. Together with the helical instability, a strong influx of impurities takes place, and it seems possible that both effects act together to amplify the disruptive effects of the instability on the discharge.

Very little can be said about the nature of the helical instability during ELMs. The fact that the mode propagates in the diamagnetic direction suggests that it is located very much on the outside of the plasma. Recently, Jakoby and Kerner[9] have proposed that pressure-driven kink instabilities, which have their resonance outside the plasma, are unstable for ASDEX pressure profiles. The

experimentally observed growth rate of about 100 μs seems considerably longer than that which would be predicted for these almost ideal MHD instabilities. A scan of the pressure gradient near the plasma edge versus poloidal magnetic field on DIII-D[10] has provided an indication that ideal ballooning modes are responsible for ELMs. Although it is not completely clear to us what sort of poloidal profile is predicted by theory for these instabilities, the fact that no large poloidal amplitude variations are seen around the torus would seem to point against ballooning modes. Moreover, it seems unlikely that ballooning instabilities are responsible for ELMs because many H-mode discharges, in particular those with grassy ELMs, are far from the β limit. Toi suggests ∇j_ϕ driven tearing modes as a cause for this instability, however, it is not clear why an instability would occur during the L phase, when the gradient of the current density near the plasma edge is small. Since the H mode and the ELMs, are seen preferentially in divertor tokamaks, it seems to us that a realistic instability model would have to incorporate effects of a divertor configuration.

Acknowledgements

The support of Dr. F.Wagner and the help of the ASDEX team is gratefully acknowledged. J.Krippner provided excellent technical assistance. One of the authors (S.v.G) is grateful to the Alexander von Humboldt foundation for support.

References:

(1) K.Toi, J.Gernhardt, O.Klüber, M.Kornherr: Report of the Max Planck Institut für Plasmaphysik Garching, IPP III/135 (1988), to be published Phys. Rev. Lett.

(2) F.Wagner, G.Becker, K.Behringer, D.Campbell, A.Eberhagen et al.:Phys. Rev Lett. 49, p.1408 (1982).

(3) M. Keilhacker, G. Becker, K. Bernhardi, A. Eberhagen, M. ElShaer et al.: Plasma Physics and Controlled Fusion 26, p.49 (1984).

(4) ASDEX Team, The H-mode of ASDEX, submitted for publication to Nuclear Fusion.

(5) K.McGuire, P.Beiersdorfer, M.Bell, K.Bol, D.Boyd, et al.: Plasma Physics and Contr.Nucl.Fusion Res.(Proc.London Conf.) IAEA (Vienna) Vol. 1, p. 117 (1984)

(6) N.Ohyabu, S.Allen, N.H.Brooks, G.Bramson, K.H.Burell, et al.: "H-Mode Study in DIII-D" in Proc. 15th European Conf. Contr. Fusion and Plasma Heating, Dubrovnik (1988)

(7) O.Klüber, J.Gernhardt, K.Grassie, J.Hofmann, M.Kornherr, et al.: Proc 13 European Conf. Contr. Fusion and Plasma Heating, Schliersee, Part 1, p. 136(1986).

(8) V.G.Merezhkin: Sov. J. Plasma Phys. 4, p.152 (1978)

(9) A.Jakoby, Report of the Max Planck Institut für Plasmaphysik 6/269 (1987) (method). For results see ref.(4)

(10) P.Gohil, M. Ali Mahdavi, L.Lao, K.H.Burrell, M.S.Chu, et al.: Phys. Rev. Lett.61, p.1603 (1988).

Figure Captions:

Fig.1: Single ELM phase of discharge.(1a) Hα emission, (1b) soft X-ray emission from radius 38.5 cm, i.e. very close to the plasma edge (Foil 7.5 μm Be), (1c) B_θ-loop signal at poloidal angle $\theta = 0^o$ (i.e. midplane on outside of torus).

Fig.2: Traces from four Mirnov coils, located at the poloidal angles $\theta = +51^o, -51^o, +149.4^o$, and -149.4^o.

Fig.3: Comparison of the displacement Δ of the plasma column and the decay of the soft X-ray intensity at plasma radii r = 8.2, 32.8, 38.5, and 40.3 cm (Foil = 7.5 μm Be).

Fig.4: H-mode discharge with grassy ELMs. (4a) Hα emission, (4b) soft X-ray emission at radius r = 2.8cm, (4c) soft X-ray emission at plasma radius r = 35.8 cm, and (4d) B_θ-loop signal $\theta = 0^o$.

Fig.5: Mirnov signals for a helical perturbation with overlapping grassy ELMs. (5a) Outer loops of the poloidal array, (5b) inner loops of the poloidal array, (5c) toroidal array. The dashed curves represent modeling curves for an m=3, n=1 perturbation assuming a value 0.7 for $\beta_{pol} + l_i/2$ for the Merezhkin correction.

Fig.6: Mirnov signals for a single ELM. The solid lines are the original data. All the dashed curves are identical; they represent the averaged signal, which is thought to be produced by the horizontal motion. (6a) Outer array of Mirnov loops, (6b) inner array, (6c) toroidal array.

Fig.7: Helical instability during a single ELM. The solid curves are the difference between the original B_θ-loop data and the average for the horizontal motion. The dashed curves represent modeling calculations for an m=4, n=1 helical mode propagating in electron diamagnetic direction. (7a) Outer loops, (7b) inner loops, and (7c) toroidal loops.

Fig.8: Fast time development of a variety of signals during a single ELM. (8a) Hα emission in the divertor, (8b) CIII emission at 934 Å near the plasma boundary, (8c) USX-emission (no foil) at plasma radius 31 cm, (8d) soft X-ray emission (Foil 7.5 μm Be) at radius r = 38.5 cm. (8e) soft X-ray emission at radius r = 38.4 cm, looking through the divertor throat, (8f) Mirnov loop signal at $\theta = 17^o$.

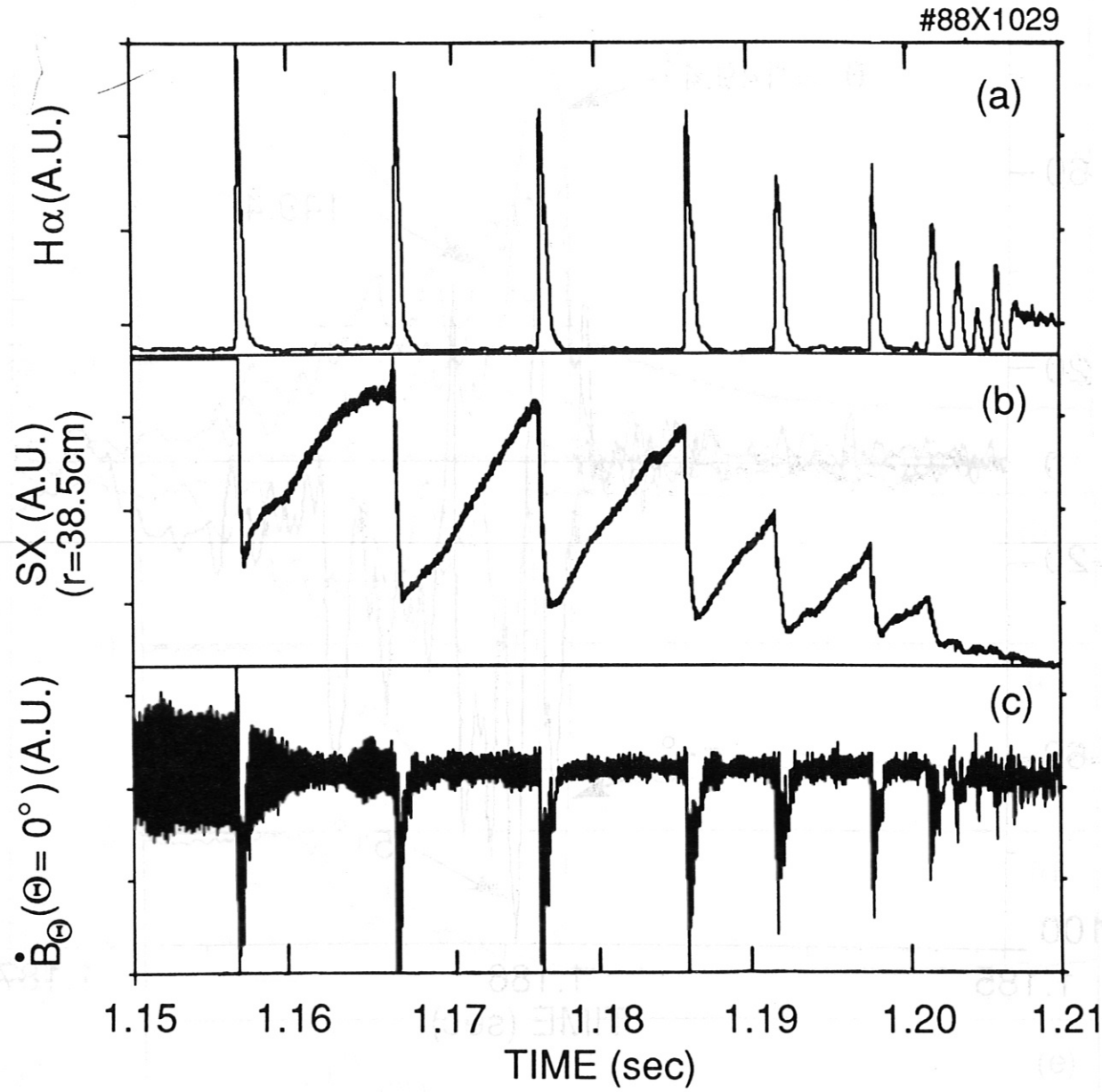
#88X1029
(a)
Hα (A.U.)
(b)
SX (A.U.)
(r=38.5cm)
(c)
$\dot{B}_\Theta$ (Θ= 0°) (A.U.)
1.15
1.16
1.17
1.18
1.19
1.20
1.21
TIME (sec)

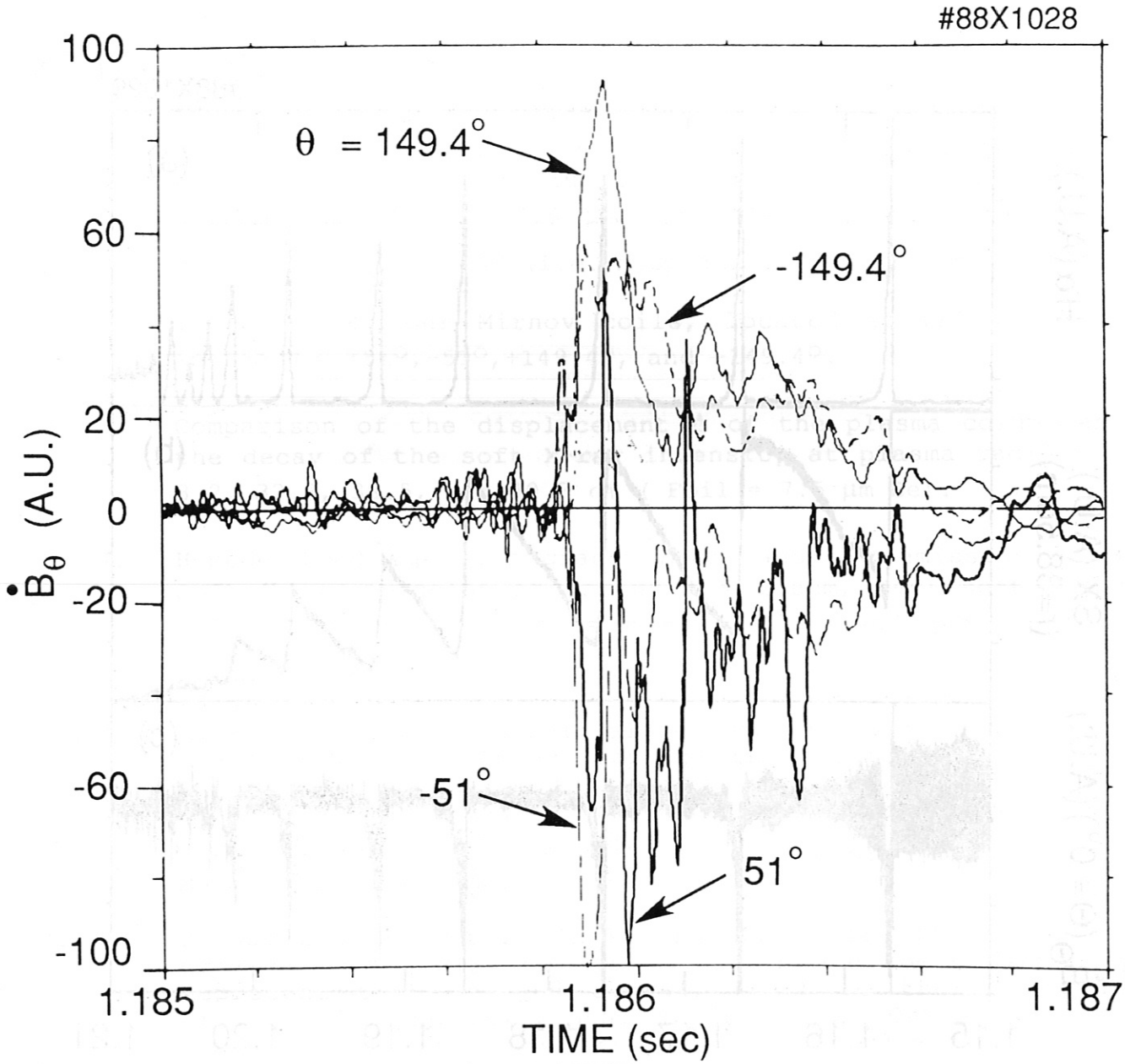
#88X1028
100
60
20
0
-20
-60
-100
θ = 149.4°
-149.4°
-51°
51°
$\dot{B}_\theta$ (A.U.)
1.185
1.186
1.187
TIME (sec)

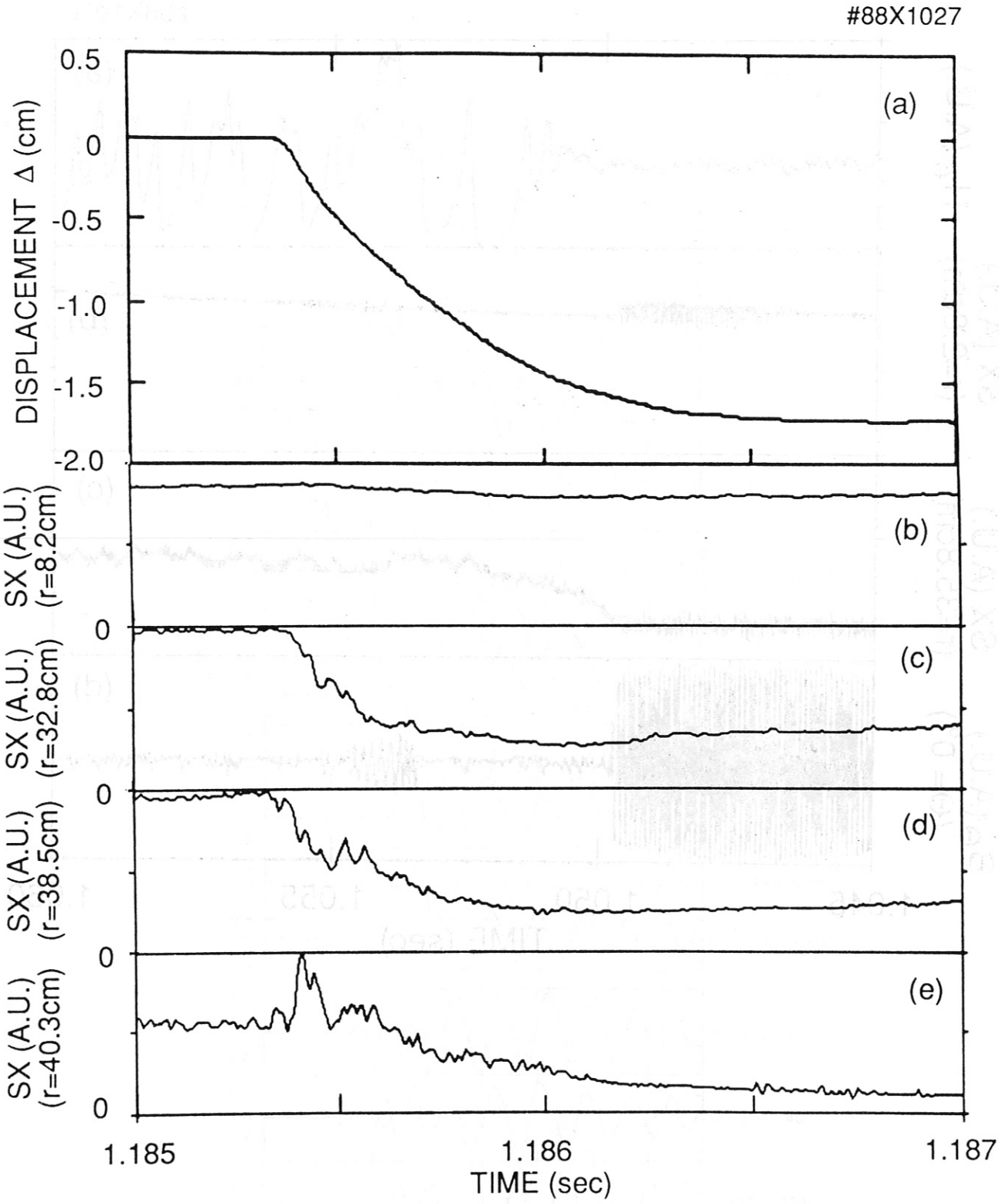
#88X1027
DISPLACEMENT Δ (cm)
0.5
0
-0.5
-1.0
-1.5
-2.0
(a)
SX (A.U.) (r=8.2cm)
(b)
SX (A.U.) (r=32.8cm)
(c)
SX (A.U.) (r=38.5cm)
(d)
SX (A.U.) (r=40.3cm)
(e)
0
1.185
1.186
1.187
TIME (sec)

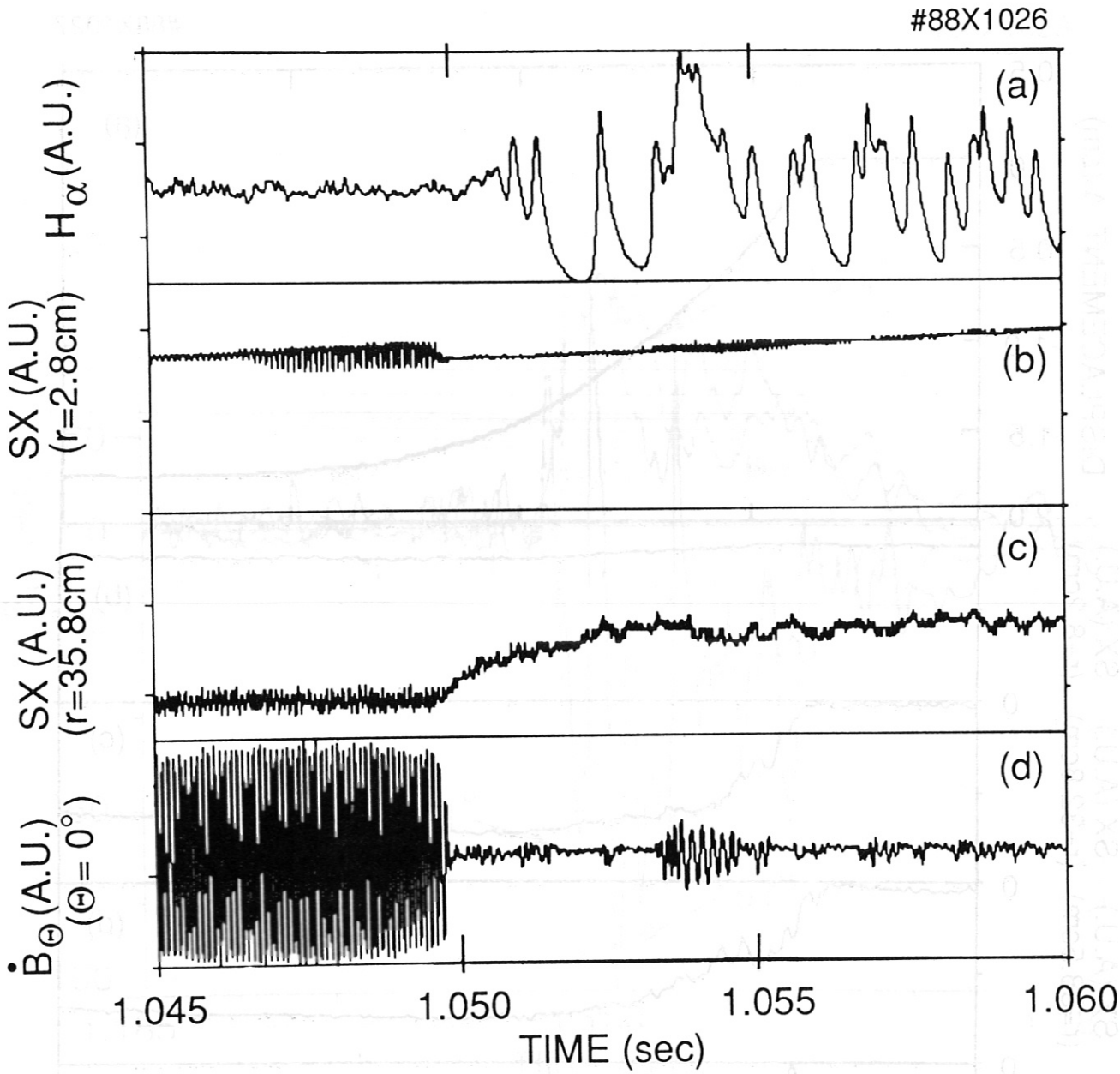
#88X1026
(a)
H_α (A.U.)
(b)
SX (A.U.) (r=2.8cm)
(c)
SX (A.U.) (r=35.8cm)
(d)
$\dot{B}_\Theta$ (A.U.) (Θ= 0°)
1.045
1.050
1.055
1.060
TIME (sec)

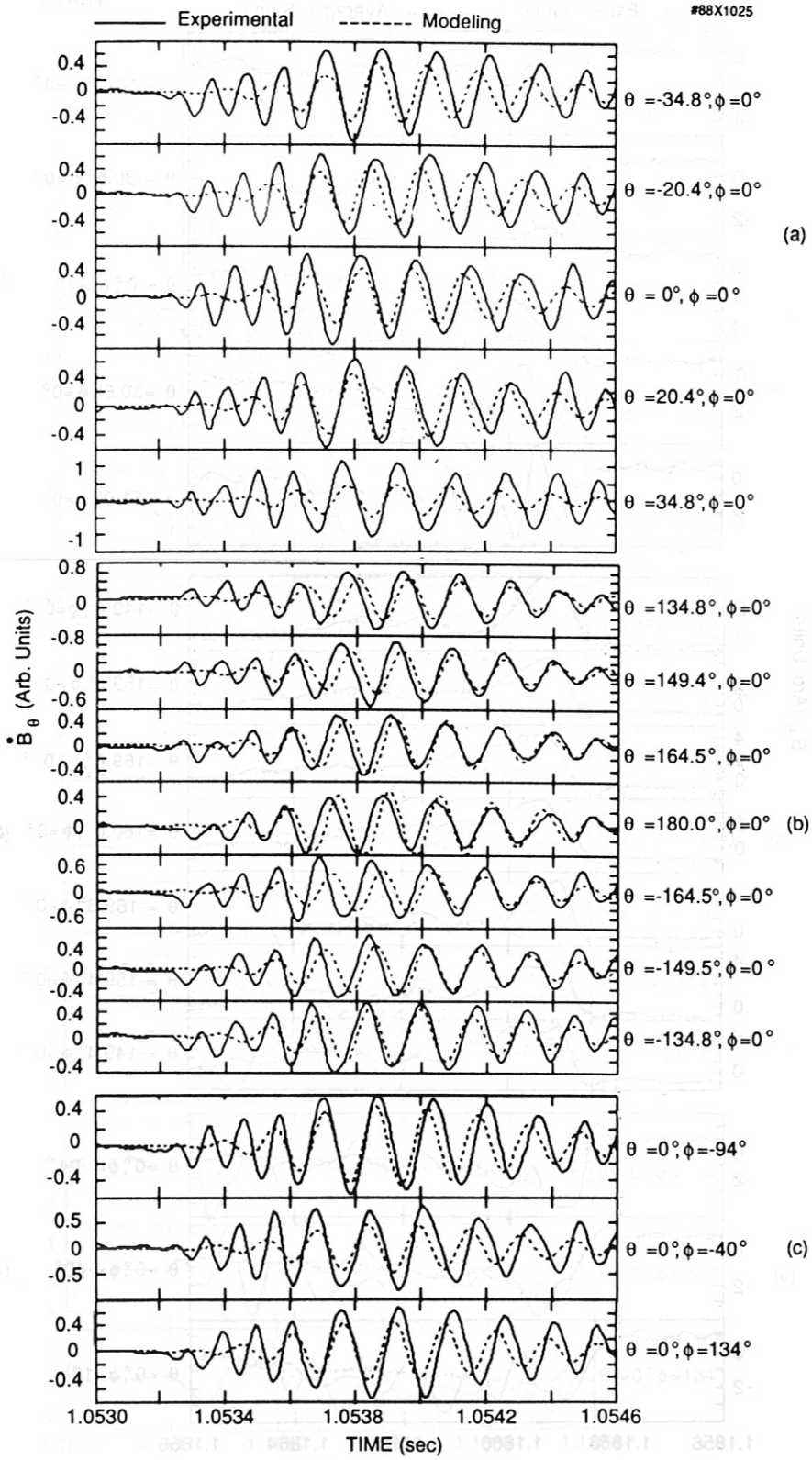
Experimental
Modeling
#88X1025
θ =-34.8°,ϕ =0°
θ =-20.4°,ϕ =0°
θ = 0°, ϕ =0°
θ =20.4°,ϕ =0°
θ =34.8°,ϕ =0°
(a)
θ =134.8°, ϕ=0°
θ =149.4°, ϕ=0°
θ =164.5°, ϕ=0°
θ =180.0°, ϕ=0°
θ =-164.5°,ϕ =0°
θ =-149.5°,ϕ =0 °
θ =-134.8°,ϕ =0°
(b)
θ =0°,ϕ =-94°
θ =0°,ϕ =-40°
θ =0°,ϕ =134°
(c)
$\dot{B}_\theta$ (Arb. Units)
1.0530
1.0534
1.0538
1.0542
1.0546
TIME (sec)

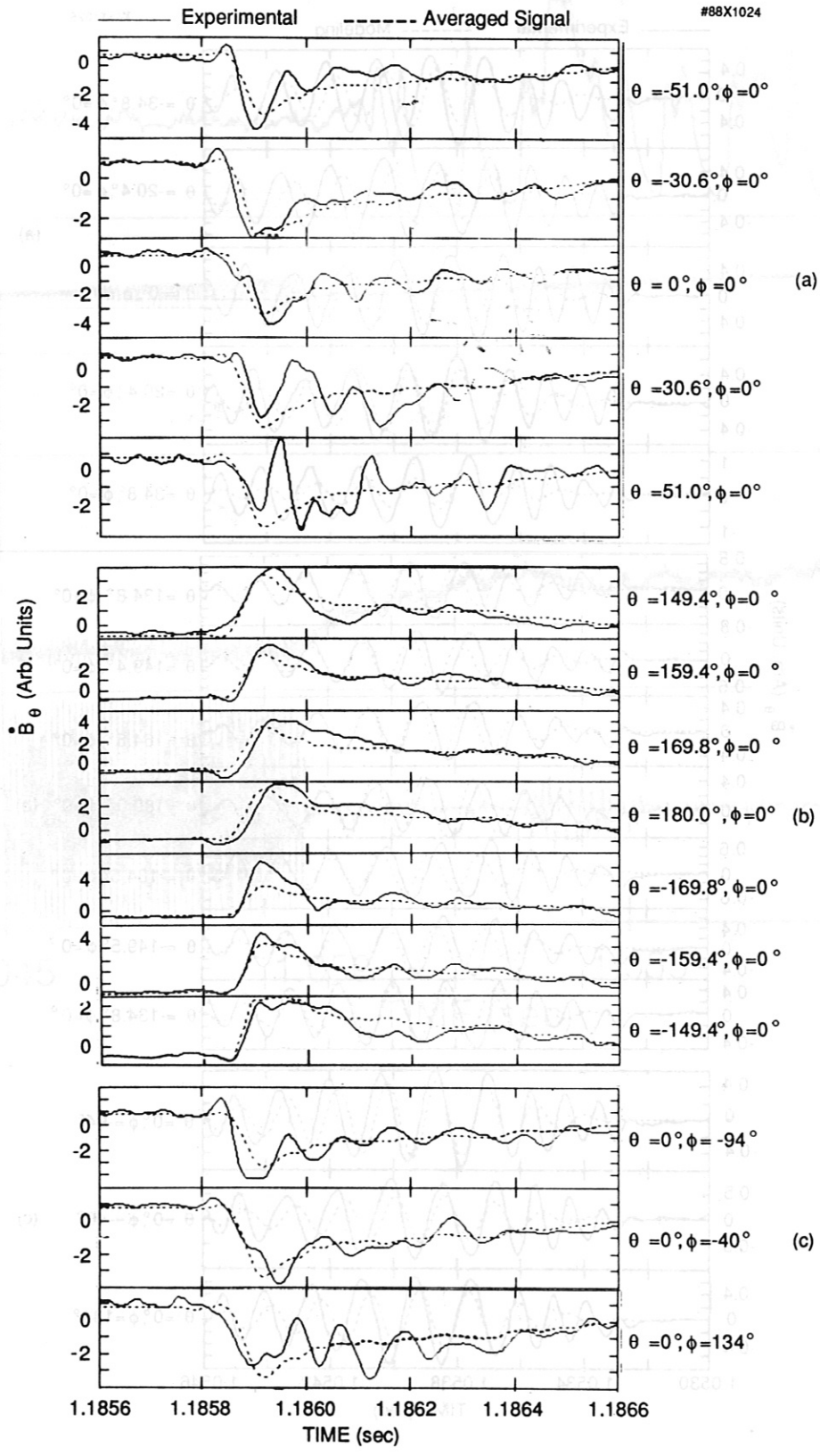
Experimental
Averaged Signal
#88X1024
θ =-51.0°,ϕ=0°
θ =-30.6°,ϕ=0°
θ = 0°, ϕ =0°
(a)
θ =30.6°,ϕ=0°
θ =51.0°,ϕ=0°
θ =149.4°, ϕ=0 °
θ =159.4°,ϕ=0 °
θ =169.8°,ϕ=0 °
θ =180.0°, ϕ=0°
(b)
θ =-169.8°, ϕ=0°
θ =-159.4°,ϕ=0 °
θ =-149.4°,ϕ=0 °
θ =0°,ϕ= -94 °
θ =0°,ϕ=-40°
(c)
θ =0°,ϕ=134°
$\dot{B}_\theta$ (Arb. Units)
1.1856
1.1858
1.1860
1.1862
1.1864
1.1866
TIME (sec)

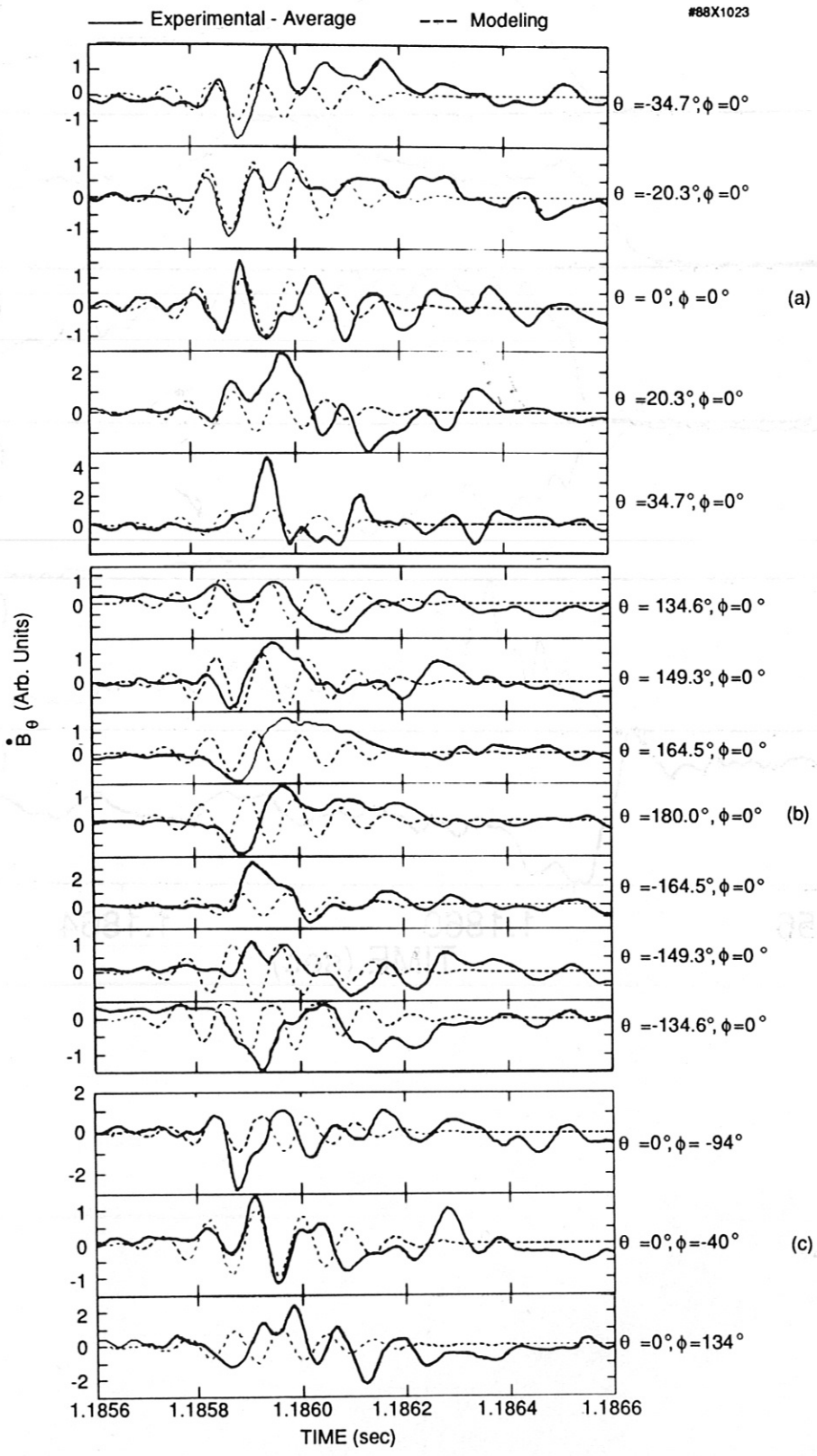
Experimental - Average
Modeling
#88X1023
θ =-34.7°,ϕ =0°
θ =-20.3°,ϕ =0°
θ = 0°, ϕ =0°
(a)
θ =20.3°,ϕ=0°
θ =34.7°,ϕ=0°
θ = 134.6°,ϕ=0°
θ = 149.3°,ϕ=0°
θ = 164.5°,ϕ=0°
θ =180.0°,ϕ=0°
(b)
θ =-164.5°,ϕ=0°
θ =-149.3°,ϕ=0°
θ =-134.6°,ϕ=0°
θ =0°,ϕ= -94°
θ =0°,ϕ=-40°
(c)
θ =0°,ϕ=134°
$\dot{B}_\theta$ (Arb. Units)
1.1856
1.1858
1.1860
1.1862
1.1864
1.1866
TIME (sec)

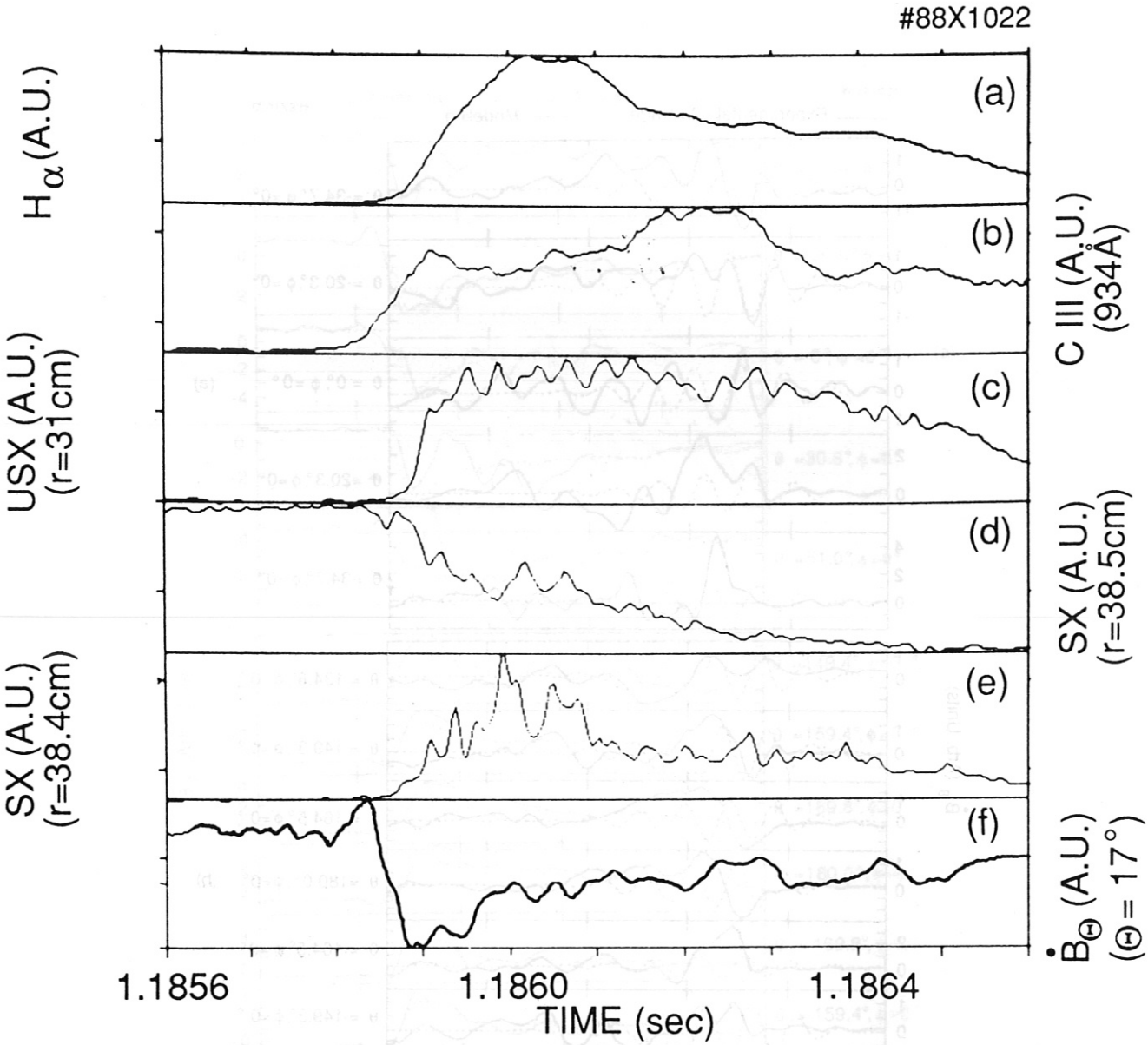
#88X1022
(a)
(b)
(c)
(d)
(e)
(f)
H_α (A.U.)
USX (A.U.) (r=31cm)
SX (A.U.) (r=38.4cm)
C III (Å.U.) (934Å)
SX (A.U.) (r=38.5cm)
$\dot{B}_\Theta$ (A.U.) (Θ = 17°)
1.1856
1.1860
1.1864
TIME (sec)